ORIGINAL ARTICLE

Appearance of remodelled and dendritic cell-rich alveolar-lymphoid interfaces provides a structural basis for increased alveolar antigen uptake in chronic obstructive pulmonary disease

Michiko Mori,[1] Cecilia K Andersson,[2] Kaj A Svedberg,[1] Pernilla Glader,[2,3] Anders Bergqvist,[2] Medya Shikhagaie,[1] Claes-Göran Löfdahl,[2] Jonas S Erjefält[1,2]

▶ Additional material is published online only. To view please visit the journal online (http://dx.doi.org/10.1136/thoraxjnl-2012-202879).

[1]Department of Experimental Medical Science, Lund University, Lund, Sweden
[2]Department of Respiratory Medicine and Allergology, Lund University Hospital, Lund, Sweden
[3]Respiratory Medicine and Allergology at Sahlgrenska Academy, University of Gothenburg, Gothenburg, Sweden

Correspondence to
Dr Jonas S Erjefält, Head, Unit of Airway Inflammation and Immunology, Department of Experimental Medical Science, BMC D12, Klinikgatan 30, Lund University, Lund SE-22184, Sweden; Jonas.Erjefalt@med.lu.se

Received 16 October 2012
Revised 6 January 2013
Accepted 16 January 2013
Published Online First 14 February 2013

ABSTRACT

Rationale The alveolar pathology in chronic obstructive pulmonary disease (COPD) involves antigen-driven immune events. However, the induction sites of alveolar adaptive immune responses have remained poorly investigated.

Objectives To explore the hypothesis that interfaces between the alveolar lumen and lymphoid aggregates (LAs) provide a structural basis for increased alveolar antigen uptake in COPD lungs.

Methods Lung samples from patients with mild (Global Initiative for Chronic Obstructive Lung Disease (GOLD) stage I), moderate–severe (GOLD II–III), and very severe (GOLD IV) COPD were subjected to detailed histological assessments of adaptive immune system components. Never smokers and smokers without COPD served as controls.

Results Quantitative histology, involving computerised three-dimensional reconstructions, confirmed a rich occurrence of alveolar-restricted LAs and revealed, for the first time, that the vast majority of vascular or bronchiolar associated LAs had alveolar interfaces but also an intricate network of lymphatic vessels. Uniquely to COPD lungs, the interface epithelium had transformed into a columnar phenotype. Accumulation of langerin $(CD207)^+$ dendritic cells occurred in the interface epithelium in patients with COPD but not controls. The antigen-capturing capacity of langerin$^+$ dendritic cells was confirmed by increased alveolar protrusions and physical T cell contact. Several of these immune remodelling parameters correlated with lung function parameters.

Conclusions Severe stages of COPD are associated with an emergence of remodelled and dendritic cell-rich alveolar–lymphoid interfaces. This novel type of immune remodelling, which predicts an increased capacity to respond to alveolar antigens, is suggested to contribute to aggravated inflammation in COPD.

Key messages

What is the key question?

- Can peripheral lymphocyte-rich lymphoid aggregates in patients with chronic obstructive pulmonary disease (COPD) provide a structural basis for alveolar antigen uptake in the peripheral lung?

What is the bottom line?

- Severe stages of COPD are associated with remodelling of the interfaces between the alveolar lumen and lymphoid aggregates. These changes, which include a selective accumulation of dendritic cells to the interface epithelium, correlate with lung function and are suggested to increase the lung's capacity to respond to alveolar immune triggers.

Why read on?

- This novel type of structural alteration is likely to contribute to the induction of adaptive immune responses in patients with advanced stages of COPD and may also represent a general adaptation to facilitate antigen uptake in the distal lung.

INTRODUCTION

Chronic obstructive pulmonary disease (COPD) is one of the leading causes of morbidity and mortality worldwide.[1] Long-term exposure to inhaled chemical irritants in tobacco smoke results in a chronic and destructive inflammation in the lung.[2 3] Apart from innate immune responses in COPD, it is becoming increasingly clear that antigen-driven adaptive immune responses are activated in COPD lungs.[4]

In conducting airways, epithelial dendritic cells (DCs) extend cytoplasmic protrusions to sample luminal antigens.[5] When an antigen is encountered, DCs migrate to draining lymph nodes and present the antigen to naïve T cells, thus initiating adaptive immune responses.[6] Importantly, adaptive immune responses in COPD also take place locally within the lungs as demonstrated by the presence of bronchiolar-associated lymphoid aggregates.[7] Since only scarce numbers of such lymphoid aggregates (LAs) are present in healthy subjects, these structures are thought to develop as a result of extended periods of inflammation or infections (ie, lymphoid neogenesis).[8–10] Consequently lung LAs are not regarded as an integral part of secondary lymphoid organs (eg, lymph nodes or Peyer's patches in the

To cite: Mori M, Andersson CK, Svedberg KA, *et al*. *Thorax* 2013;**68**:521–531.

intestines) and are therefore called tertiary lymphoid organs or ectopic lymphoid tissues.[10]

Lung LAs may acquire inhaled luminal antigens via migration of superficial airway DCs.[11] However, LAs have also been observed at sites distant from the conducting airways.[12–14] It remains unclear whether or not these structures acquire luminal antigens from other lung regions such as the alveolar parenchyma, a compartment that in COPD is frequently subjected to inflammation and infections.[15] However, although alveolar adaptive immune responses are likely to occur extensively in COPD, little is known about how and where the alveolar antigen uptake takes place.

Recent experiments in mice show that when antigen is instilled into the lungs, most of the total antigen uptake is carried out by scattered DCs in the alveolar parenchyma.[16 17] However, it can be speculated that in human airway diseases, such as COPD, alveolar antigen uptake is also carried out at specialised alveolar–lymphoid interfaces, similar to the luminal–lymphoid interfaces in classical mucosal-associated lymphoid tissues. However, despite such an arrangement facilitates a localised and more rapid antigen presentation, alveolar–lymphoid interfaces have never been explored previously. This study performs the first focused exploration of this interface and tests the hypothesis that DC-rich interfaces between the alveolar lumen and LAs provide a structural basis for increased alveolar antigen uptake in COPD.

METHODS

Additional methodological details are provided in the online supplementary data.

Patients

Lung tissue from patients with COPD and never-smoking and smoking controls was collected from 46 subjects undergoing lung transplantation or surgical resection for suspected lung cancer.[18] The patients with COPD were divided into mild (Global Initiative for Chronic Obstructive Lung Disease (GOLD) stage I), moderate to severe (GOLD II–III) and very severe (GOLD IV) COPD. The subject characteristics, inclusion criteria and methodological details, are presented in table 1 and in the online supplementary data.

All subjects gave written informed consent to participate in the study, which was approved by the local ethics committee.

Characterisation of peripheral lung LAs

For each subject multiple peripheral lung samples were subjected to standardised fixation and processing for generating paraffin sections. LAs, defined as more than 50 contiguous lymphoid cells, were quantified and subgrouped according to their anatomical location: small airway/bronchiolar-associated lymphoid tissue (abbreviated BRALT in order to make a distinction to bronchial-associated lymphoid tissue BALT), vascular-associated lymphoid tissue (VALT, defined as LAs in non-bronchiolar-associated solitary vessels with a diameter >140 μm) and alveolar-only lymphoid tissue (ALT, defined as LAs well separated from any bronchioles, pleural tissue or pulmonary vessels).

Immunohistochemistry

Immunohistochemistry (IHC) was performed in an automated IHC robot (DakoCytomation, Glostrup, Denmark). All primary antibodies used (see table 2) and IHC protocols have been validated extensively for use on paraffin sections.

The immunoreactivity was visualised using the Dako EnVision kit.[19] For bright field double staining the first primary antibody was detected with horseradish peroxidase-conjugated antibodies and the second with alkaline phosphatase-conjugated

Table 1 Subject characteristics

Characteristic	Never smokers	Smokers w/o COPD	GOLD I COPD	GOLD II–III* COPD	GOLD IV COPD
Subjects, n	8	7	6	15	10
Gender, men/women	2/6	3/4	4/2	12/3	4/6
Age, years	66 (33–76)†	56 (47–68)	68 (56–75)	67 (53–77)	62 (53–66)
Smoking history, pack-years	0	36 (20–80)	39 (25–66)	46 (16–65)	43 (25–60)
Smoking status, ex smokers/current	–	3/4	3/3	10/5	10/0
FEV_1	2.5 (1.7–5.1)	3.0 (1.9–3.5)	2.9 (1.6–3.2)	1.9 (1.2–2.9)	0.6 (0.4–1.0)
FEV_1, % of predicted	108.9 (82–141)	95.0 (82–120)	85.9 (80–95)	68.5 (43–78)	23.1 (15–27)
FEV_1/(F)VC, %	81.5 (66–121)	76.0 (71–88)	66.5 (65–70)	58.0 (41–68)	32.0 (20–39)
Inhaled β_2 agonists					
Short acting (yes/no/unknown)	0/8/0	0/7/0	1/5/0	2/13/0	4/5/1‡
Long acting (yes/no/unknown)	0/8/0	0/7/0	0/6/0	0/15/0	4/5/1‡
Inhaled anticholinergics					
Short acting (yes/no/unknown)	0/8/0	0/7/0	1/5/0	2/13/0	3/6/1‡
Long acting (yes/no/unknown)	0/8/0	0/7/0	0/6/0	0/15/0	5/4/1‡
Inhaled short acting β_2 agonist plus anticholinergics (yes/no/unknown)	0/8/0	0/7/0	0/6/0	0/15/0	3/6/1‡
Corticosteroids					
Inhaled (yes/no/unknown)	0/8/0	0/7/0	0/6/0	1/14/0	2/7/1‡
Oral (yes/no/unknown)	0/8/0	0/7/0	0/6/0	0/15/0	2/7/1‡
Inhaled long acting β_2 agonist plus corticosteroids (yes/no/unknown)	0/8/0	0/7/0	0/6/0	1/14/0	7/2/1‡
Mucolytics (yes/no/unknown)	0/8/0	0/7/0	2/4/0	0/15/0	5/4/1‡

Values are median (range) or n.
*Two patients with GOLD stage III COPD.
†The mean value of the study group is 63 years.
‡One patient with unknown medical history.
COPD, chronic obstructive pulmonary disease; FEV_1, forced expiratory volume in 1 s; (F)VC, (forced) vital capacity; GOLD, Global Initiative for Chronic Obstructive Lung Disease.

Table 2 Primary antibodies used for immunohistochemistry

Antigen	Clone*	Supplier	Antigen retrieval	Dilution†	Against
CD20	L26	Dako, Glostrup, Denmark	Low pH‡ PT	1:1200 1:600 (IF)	B cells
CD4	1F6	Novocastra§, Newcastle Upon Tyne, UK	Low pH‡ PT	1:50	T-helper cells
CD11c	5D11	Novocastra§	Low pH‡ PT	1:100	Macrophages and myeloid dendritic cells
CD68	PG-M1	Dako	Low pH‡ PT	1:500	Monocytes and macrophages
CD21	1F8	Dako	Low pH¶ PC	1:100	Follicular dendritic cells
BDCA-2	104C12.08	Dendritics, Lyon, France	Low pH** PC	1:50	Plasmacytoid dendritic cells
Multi-Cytokeratin	AE1/AE3	Novocastra§	Low pH‡ PT	1:300 1:150 (IF)	Epithelial cells
Ki-67	Rabbit polyclonal	Biocare Medical, Concord, CA, USA	Low pH** PC	1:200	Cell proliferation
Langerin (CD207)	12D6	Novocastra§	Low pH‡ PT	1:100 1:80 (IF)	Langerhans-like dendritic cells
Podoplanin	D2–40	Biocare Medical	Low pH** PC	1:100	Lymphatic endothelium
α-Smooth muscle actin	1A4	Sigma-Aldrich, St Louis, MO, USA	Low pH** PC	1:1000	Smooth muscle cells

*Mouse monoclonal antibodies unless otherwise stated.
†Working dilution for bright field staining, unless otherwise stated.
‡EnVision FLEX Target Retrieval Solution, pH 6.1, K8005, Dako.
§Distributed by Leica Biosystems Newcastle, UK.
¶S1700, pH 6.1, Dako.
**DIVA Decloaker, pH 6, DV2004 MX, Biocare Medical.
IF, immunofluorescence; PC, pressure cook, 2100 Retriever, Prestige Medical Ltd., Blackburn, England; PT, pre-treatment module, Dako, Glostrup, Denmark.

antibodies. Immunofluorescence double staining was performed to evaluate colocalisation.[18]

Serial section-based three-dimensional reconstruction of LAs

A series of serial sections (>30) was used to generate image segmentation data of LAs, parenchymal tissue and immunostained lymphatic vessels. Structure-specific segmentation data were loaded into a software platform (Amira 5.4.2 Visage Imaging Inc, San Diego, California, USA) to reveal the three-dimensional structure.

Quantifications

For each subject multiple large sections (from two to three separated peripheral lung regions) were analysed. High-resolution digital images, representing the entire section area, were generated from all bright field sections using a slide-scanning robot (ScanScope, Aperio Technologies, Vista, California, USA). Morphometric analyses and quantification of immunoreactivity were performed using Aperio ImageScope V.10.0 software (Aperio Technologies). Apart from multiple alveolar regions, a total of around 1000 individual bronchioles and pulmonary vessels were evaluated. Alveolar–LA interfaces were measured by manual cursor tracing. Langerin$^+$ DCs were manually counted along alveolar–LA interfaces and in distinct regions within the LAs. Quantifications involving manual counting or cursor tracing were performed on blinded sections.

Statistics

Values are given as median (range), unless otherwise stated. The Kruskal–Wallis non-parametric test followed by Dunn's multiple comparisons post test was used for comparison between study groups and the Mann–Whitney test was used for comparisons between two groups (Prism V.5.0, GraphPad Software, San Diego, California, USA). Spearman's rank method was used to calculate correlation coefficients.

RESULTS

LAs are present in all major peripheral lung compartments

Two-dimensional approach to assess the distribution of LAs

Prompted by initial observations of a widespread anatomical distribution of LAs in COPD lungs (see online supplementary figure S1 and table S1), all LAs were quantified and divided into BRALTs, VALTs and ALTs (figure 1A, see online supplementary figure S1 and table S1). The BRALT structures were mainly observed in the adventitia layer of the bronchioles. Across all study groups an average of 17.7% of the BRALTs reached the bronchiolar epithelium. Although the percentage of bronchioles containing BRALTs was increased in GOLD stage IV COPD compared with never smokers ($p<0.05$), the number of BRALTs was not changed among the study groups. The number of VALTs, which had an almost exclusive adventitial distribution, increased in patients with GOLD stage IV COPD compared with never-smoking control subjects ($p<0.01$). In the alveolar parenchyma, patients with COPD displayed a tendency to increased number of ALTs (see online supplementary table S1). In GOLD stage IV, most LAs were well developed as indicated by Ki-67$^+$ proliferating cells and increased CD21$^+$ follicular DCs (see online supplementary data). Follicular CD21 immunoreactivity was observed equally frequently among BRALTs, VALTs and ALTs.

Three-dimensional confirmation of true alveolar-only LAs

A serial section-based three-dimensional analysis was performed to reveal the true spatial distribution of the lung LAs. This analysis confirmed the presence of true ALT structures; that is, alveolar-only LAs without physical contact with bronchioles or pulmonary vessels (figure 1B–D). In COPD, an average of 25.4% of all LAs were true ALTs and 31.2% of all LAs were VALTs. Consequently, the remaining 43.4% of the LAs were BRALTs. This serial section analysis also revealed that 79.8% of all identified ALTs in two-dimensional sections were in fact true ALTs. Similarly, 89.3% of all VALTs were true VALTs.

BRALT and VALT structures have extensive interfaces with the alveolar lumen and the lymphatics

The vast majority of the LAs, including BRALTs and VALTs, had a direct interface towards the alveolar lumen (figure 2A,C,D).

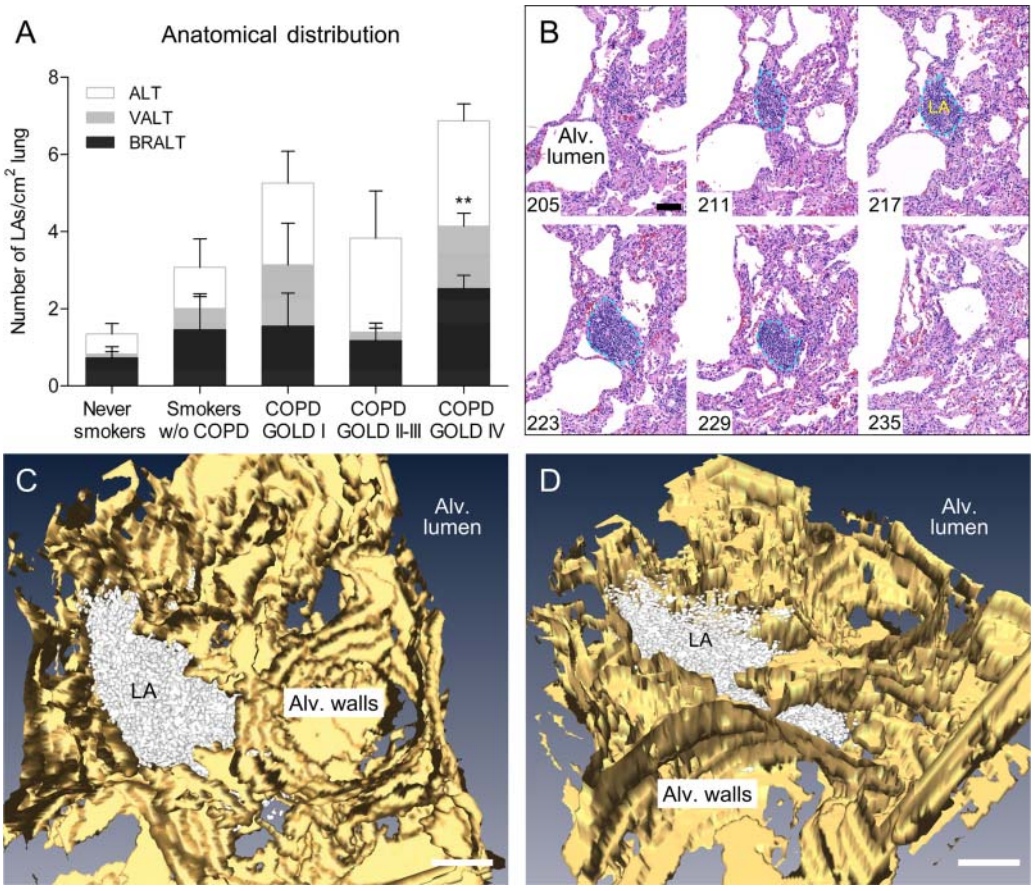

Figure 1 Lymphoid aggregates (LAs) are formed in all major lung compartments of the peripheral lung. (A) Bar graph showing the relative proportion of alveolar-only lymphoid tissue (ALT), vascular-associated lymphoid tissue (VALT), and bronchiolar-associated lymphoid tissue (BRALT) structures, as revealed by two-dimensional analysis of Masson's trichrome-stained sections from never smokers, smokers without chronic obstructive pulmonary disease (COPD) and patients with Global Initiative for Chronic Obstructive Lung Disease (GOLD) stage I–IV COPD. Values are given as mean±SEM. Statistical analysis was performed using the Kruskal–Wallis non-parametric test followed by Dunn's multiple comparison post test. **p<0.01. (B) Examples from a series with >400 haematoxylin-eosin stained sections (4 μm thick) used to reveal the true three-dimensional distribution of peripheral lung LAs. The images exemplify the gradual emergence and disappearance of a LA (outlined by dashed lines) without any associated pulmonary vessel or conducting airway. The section number is indicated in the images. (C) Similar image stacks were used to visualise true alveolar LA by computerised three-dimensional reconstruction, exemplified by a LA (white) and surrounding parenchymal tissue (yellow) and alveolar lumen (blue grey) (see online supplementary data for methodological details). (D) Three-dimensional image of another viewing angle. Scale bars: (B) 100 μm; (C,D) 200 μm.

Irrespective of anatomic location, no difference in the frequency of LAs with alveolar interfaces was found between the study groups (figure 2A and table 3).

The total length of alveolar interfaces, which is the combination of LA numbers and mean length of alveolar interfaces, was increased in advanced COPD compared with never-smoking controls (figure 2B). Among all LAs and study groups, an average of 33.4% of the LA perimeter was facing alveolar lumen (figure 2F).

Immunohistochemical visualisation of podoplanin$^+$ lymphatic vessels demonstrated a close spatial relationship between LAs and lymphatics (figure 2C,D). Three-dimensional reconstruction of podoplanin-stained lymphatic vessels further revealed the intricate connection among BRALT, VALT, ALT and lymphatics (exemplified in figure 2E). Across all study groups lymphatic vessels comprised an average of 20.3% of the LA perimeter (figure 2F).

Remodelling of alveolar–lymphoid interface epithelium in COPD

In never-smoking controls the alveolar–lymphoid epithelium was, at all locations, primarily of a simple squamous type (figure 3A,E). A similar epithelium, but with increasing stretches of cuboidal epithelium, was present in smokers and patients with COPD (figure 3B,F). At more advanced stages of COPD (GOLD II–IV) the occurrence of cuboidal epithelium was accompanied by a higher columnar, non-ciliated epithelium (figure 3G,H). The emergence of columnar epithelium occurred similarly among BRALTs, VALTs and ALTs (table 3) and resulted in a significantly increased proportion and increased total columnar epithelial length in patients with GOLD IV COPD (figure 3C,D). Importantly, the columnar epithelium in patients with GOLD II–IV COPD was restricted to alveolar–LA interfaces (similar epithelium was not found in surrounding lung parenchyma or along other alveolar interfaces facing, for example, the adventitia of pulmonary vessels or conducting airways).

Selective accumulation of antigen-presenting DCs along alveolar–lymphoid interfaces in COPD lungs

Langerin (CD207)$^+$ DCs represent a major antigen-presenting cell type in the conducting airways in COPD.[20 21] Hence, we explored if langerin$^+$ DCs were present at alveolar–LA interfaces. Irrespective of anatomic location, no or very few interface langerin$^+$ DCs were present in never-smoking and smoking

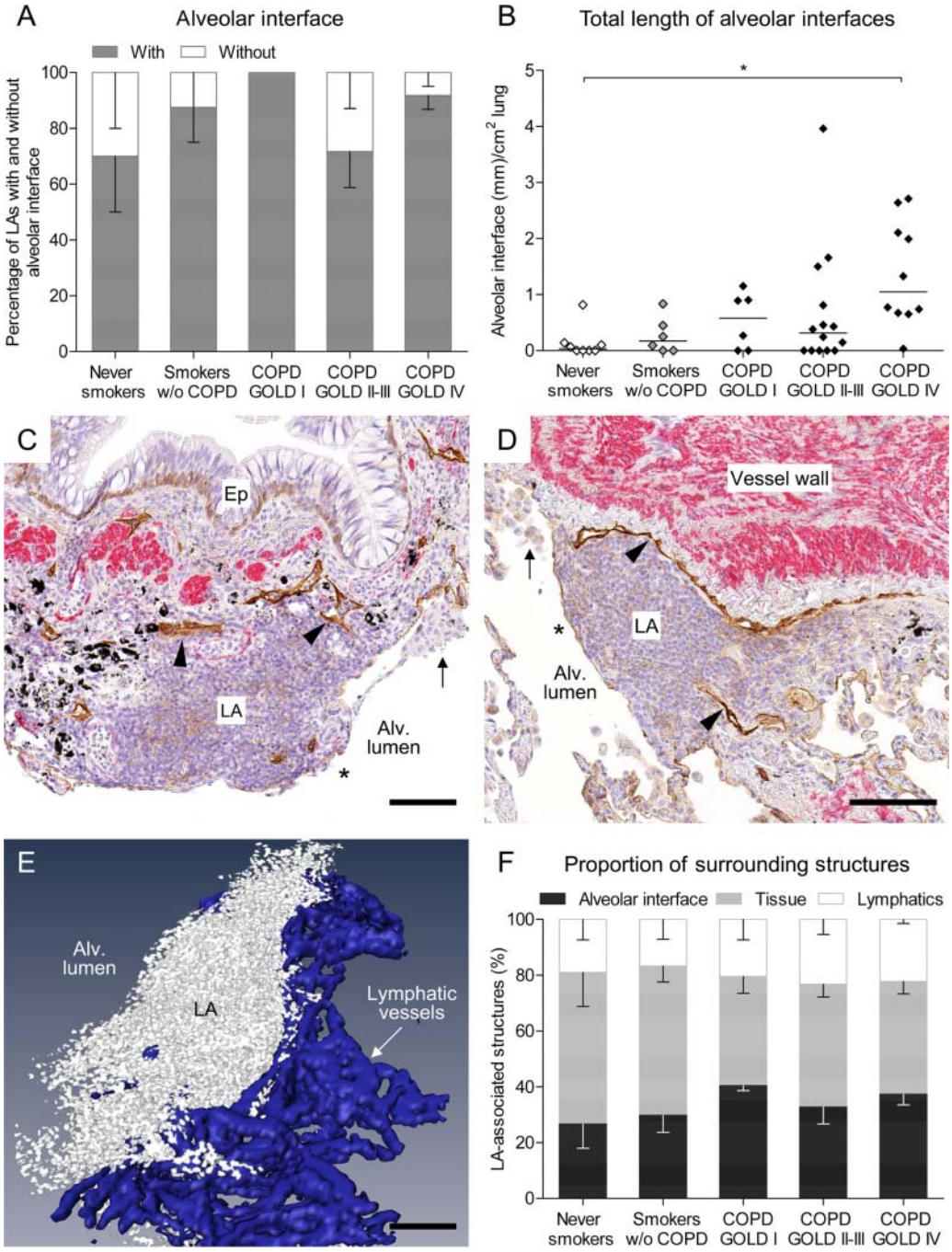

Figure 2 Lymphoid aggregates (LAs) have extensive interfaces with the alveolar lumen and peripheral lymphatic vessels. (A) Quantitative data showing that in all study groups the majority of LAs had an alveolar lumen–LA interface, irrespective of anatomical localisation. Values are given as mean±SEM. (B) Quantification of the total length of alveolar–LA interfaces. Statistical analysis was performed using the Kruskal–Wallis non-parametric test followed by Dunn's multiple comparison post test. Horizontal lines indicate medians for each group. *p<0.05. (C) Photomicrograph of a typical bronchiolar-associated lymphoid tissue (BRALT) with its interface with the alveolar lumen (asterisk) and podoplanin$^+$/α-smooth muscle actin$^+$ lymphatic vessels (arrowheads; brown). α-Smooth muscle actin$^+$ cells are shown in red. Arrow indicates alveolar macrophages and 'Ep' the bronchiolar epithelium. Black endogenous pigment depositions are also visible. Epithelial basal cells and pneumocytes showed a weak immunoreactivity for podoplanin. Cell nuclei were counterstained with Mayer's haematoxylin (blue stain). (D) Photomicrograph of a similarly stained vascular-associated lymphoid tissue (VALT) with its direct interface with the alveolar lumen and extensive connection to podoplanin$^+$/α-smooth muscle actin$^+$ lymphatic vessel (arrowheads). (E) Three-dimensional rendering of an image stack with 40 (4 μm thick) serial sections revealed an intricate relationship between immunostained lymphatic vessels and peripheral lung LA. White: LA; blue: lymphatic vessels. (F) The relative proportion of anatomic structures along the LA perimeters, divided into alveolar interface, lymphatic vessel borders and remaining firm tissue (ie, airway wall tissue, adventitial tissue of pulmonary vessels, or parenchymal tissue). Values are given as mean±SEM. Scale bars: (C–E) 100 μm.

Table 3 Characteristics of alveolar lumen–LA interfaces

Parameters	Never smokers	Smokers w/o COPD	GOLD I COPD	GOLD II–III COPD	GOLD IV COPD	Overall p value*
LAs with alveolar interfaces, %						
BRALT	50 (0–100)	50 (0–100)	100 (100–100)	100 (100–100)	100 (0–100)	0.205
VALT	NA	100 (100–100)	100 (100–100)	100 (0–100)	100 (83–100)	0.427
ALT	100 (100–100)	100 (100–100)	100 (100–100)	100 (75–100)	100 (100–100)	0.615
Simple squamous epithelium, % of total alveolar interface						
BRALT	97 (93–100)	80 (80–80)	100 (100–100)	67 (9–100)	55 (37–73)	0.077
VALT	NA	74 (74–74)	51 (0–100)	73 (57–100)	63 (0–84)	0.655
ALT	100 (84–100)	71 (53–89)	61 (10–70)	77 (40–89)	81 (56–97)	0.126
Simple cuboidal epithelium, % of total alveolar interface						
BRALT	3 (0–7)	20 (20–20)	0	17 (0–91)	26 (13–41)	0.115
VALT	NA	26 (26–26)	49 (0–100)	25 (0–43)	20 (13–100)	0.724
ALT	0 (0–16)	29 (11–47)	39 (30–90)	23 (11–60)	13 (2–36)	>0.050
Columnar epithelium, % of total alveolar interface						
BRALT	0	0	0	0 (0–65)	17 (0–40)	0.097
VALT	NA	0	0	0 (0–6)	6 (0–68)	0.141
ALT	0	0	0	0	1 (0–34)	0.089
Number of langerin$^+$ DCs per mm^2 of LA						
All LAs	87 (19–262)	50 (31–128)	141 (90–262)	113 (0–203)	147 (85–228)	0.225
BRALT	38 (37–104)	0	151 (141–161)	94 (0–218)	130 (108–254)	0.036
VALT	NA	70 (31–190)	174 (61–288)	179 (27–232)	145 (96–409)	0.508
ALT	182 (102–262)	100 (99–101)	168 (155–182)	79 (0–203)	126 (15–181)	0.256
Number of langerin$^+$ DCs per mm of total alveolar interface						
All LAs	0	0.14 (0–2.36)	2.96 (0–5.27)	2.11 (0–5.76)	3.10 (1.08–4.77)	0.031
BRALT	0	NA	0.83 (0–1.67)	0 (0–3.39)	3.03 (0.95–5.16)	0.061
VALT	NA	0 (0–3.82)	5.11 (3.21–7.02)	8.56 (0–11.86)	4.18 (1.03–8.22)	0.411
ALT	0	0.84 (0.28–1.40)	1.87 (0–3.74)	1.57 (0–9.19)	1.70 (0–4.78)	0.349
Number of langerin$^+$ DCs per mm of simple squamous interface						
BRALT	0	NA	0.54 (0–1.07)	0 (0–3.46)	0.74 (0–3.96)	0.382
VALT	NA	0	0.24 (0–0.47)	0 (0–6.81)	0 (0–2.86)	0.592
ALT	0	0	3.01 (0–6.01)	0 (0–6.45)	1.16 (0–4.93)	0.429
Number of langerin$^+$ DCs per mm of simple cuboidal interface						
BRALT	0	NA	1.89 (0–3.78)	0 (0–6.52)	1.70 (0–6.29)	0.211
VALT	NA	0 (0–5.89)	9.78 (5.81–13.74)	5.66 (0–26.06)	6.85 (0–15.71)	0.523
ALT	0	4.64 (4.18–5.09)	0	3.05 (0–13.70)	0.72 (0–7.97)	0.183
Number of langerin$^+$ DCs per mm of columnar interface						
All LAs	NA	NA	NA	5.26 (3.97–6.56)	2.10 (0–9.48)	0.178
BRALT	NA	NA	NA	2.98 (0–5.95)	3.44 (0–7.13)	1.000
VALT	NA	NA	NA	9.84 (0–19.69)	2.94 (0–24.83)	1.000
ALT	NA	NA	NA	0	0 (0–7.12)	0.422

Values are median (range).
*Kruskal–Wallis test for differences between groups or Mann–Whitney test for comparisons between two groups.
ALT, alveolar-only lymphoid tissue; BRALT, small airway/bronchiolar-associated lymphoid tissue; COPD, chronic obstructive pulmonary disease; DC, dendritic cell; GOLD, Global Initiative for Chronic Obstructive Lung Disease; LA, lymphoid aggregate; NA, not available; VALT, vascular-associated lymphoid tissue.

controls (figure 4D–F). In contrast, abundant and increased numbers of langerin$^+$ DCs were observed in COPD (figure 4D–F and table 3). No, or few such DCs were present in non-LA alveolar interfaces.

A detailed analysis of the distribution of langerin$^+$ DCs in LAs with an alveolar interface revealed a selective accumulation of DCs to the alveolar interface region. The highest density was within the alveolar interface epithelium (figures 4A and 5). Also within the lymphoid tissue, the DCs accumulated to the superficial region just beneath the alveolar interface epithelium (figure 4G). In all COPD groups the superficial LA regions had significantly higher DC densities compared with central or opposing regions (the overall p value was 0.034 for GOLD I and 0.002 for GOLD II–III and GOLD IV). The selective accumulation of interface DCs was equally present irrespective of the anatomical distribution of the LAs. In total, across the COPD groups more than 80% of the LA-associated langerin$^+$ DCs were present within the interface epithelium or in the superficial LA region (exemplified in figures 4A and 5).

The langerin$^+$ DCs within the alveolar–lymphoid epithelium frequently displayed apical protrusions reaching the alveolar border (figures 4A,B and 5A,C,D). This phenomenon was more frequent in the alveolar–LA epithelium compared with langerin$^+$ DCs along the epithelium in the conducting airways. Due to the thin interface at alveolar–LA borders, several DCs were observed with simultaneous physical contact with the alveolar surface and underlying lymphocyte populations within the LAs, including CD20$^+$ B cells and CD4$^+$ T cells (figure 5B,C). Other DC populations, such as CD68$^+$ CD11c$^+$ myeloid-like DCs or BDCA-2$^+$ plasmacytoid DCs did not have similar accumulation at the alveolar interfaces as the langerin$^+$ DCs (see online supplementary figure S3).

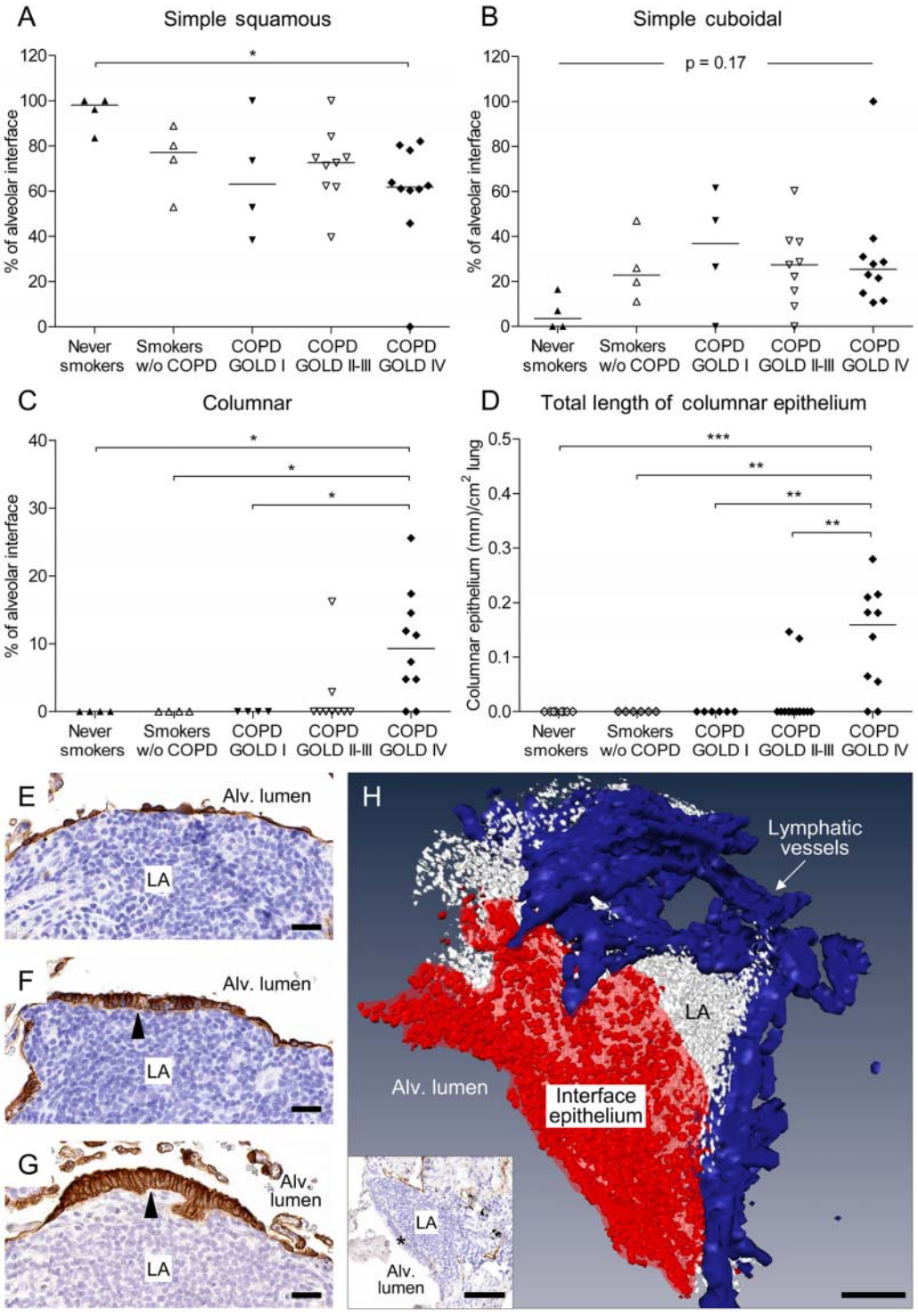

Figure 3 Altered epithelial phenotype at alveolar–lymphoid aggregate (LA) interfaces in patients with chronic obstructive pulmonary disease. The proportion of (A) simple squamous, (B) simple cuboidal and (C) columnar interface epithelium was quantified on podoplanin (lymphatic vessels)/ α-smooth muscle actin stained-sections from peripheral lung samples. (D) Quantification of the total length of columnar interface epithelium. (A–D) Statistical analyses were performed using the Kruskal–Wallis non-parametric test followed by Dunn's multiple comparison post test. Horizontal lines indicate medians for each group. *p<0.05; **p<0.01; ***p<0.001. (E–G) Micrographs where brown cytokeratin immunoreactivity visualise the epithelium at alveolar–LA interfaces. Representative images of (E) a simple squamous epithelium; (F) a simple cuboidal epithelium (arrowhead) surrounded by squamous epithelium; (G) a patchy stretch of non-ciliated columnar epithelium (arrowhead, note the sharp border to the flanking squamous epithelium). Cell nuclei were counterstained with Mayer's haematoxylin (blue stain). (H) Computerised three-dimensional rendering of podoplanin-stained sections demonstrated the functional spatial arrangement between the alveolar lumen and interface epithelium (red), the LA (white) and the opposing intertwined network of lymphatic vessels (blue). The inset exemplifies an image from the series with 40 (4 μm thick) podoplanin-stained sections used for the three-dimensional reconstruction (see online supplementary data for methodological details). The asterisk indicates the interface epithelium. Scale bars: (E–G) 25 μm; (H, inset) 100 μm.

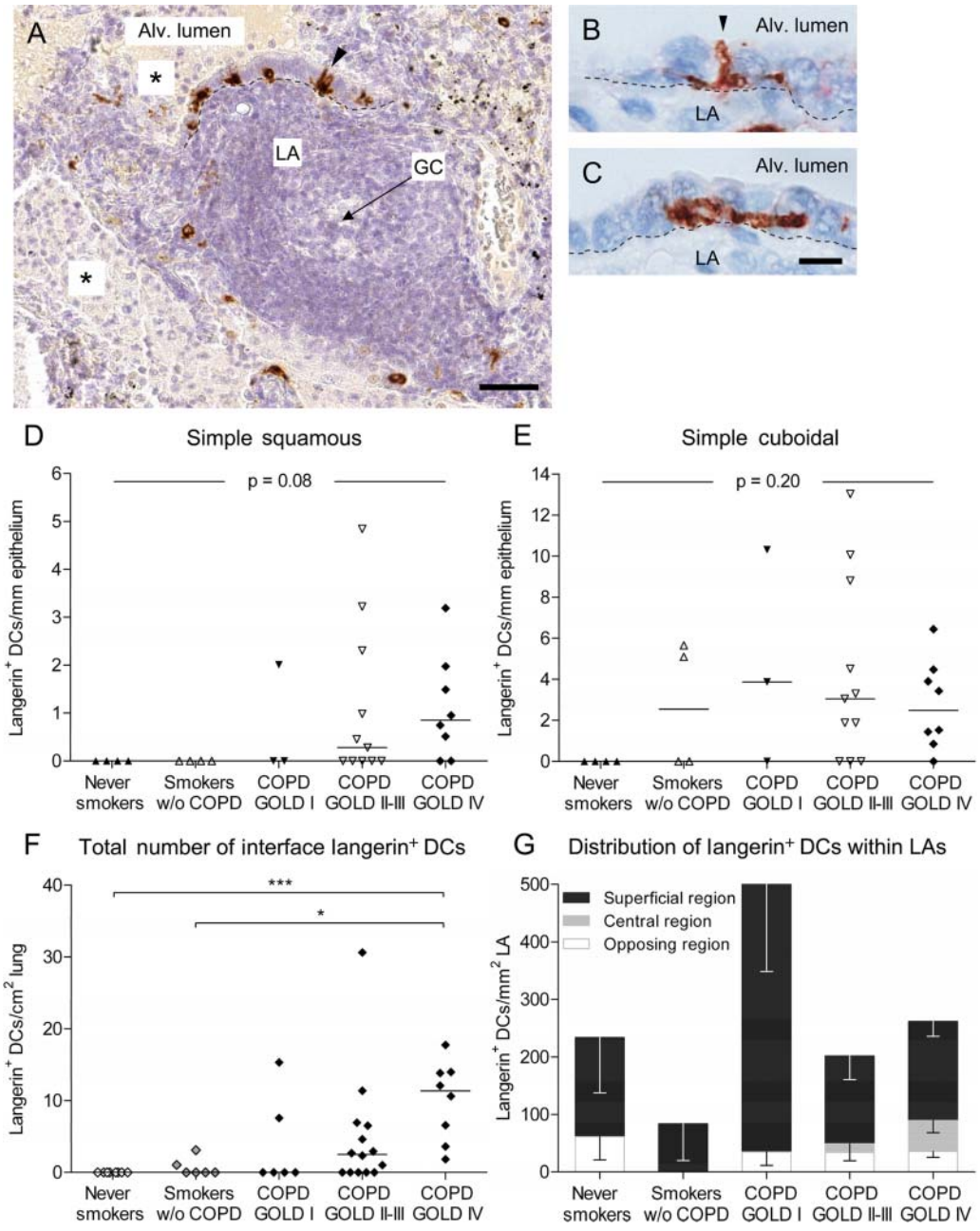

Figure 4 Accumulation of langerin$^+$ dendritic cells (DCs) along alveolar–lymphoid aggregate (LA) interfaces. (A) Micrograph exemplifying homing of langerin$^+$ DCs (brown) along the interface epithelium overlying a LA with a germinal centre (GC) (scale bar, 50 μm). Asterisks indicate alveolar lumen filled with macrophages. Arrowhead points to a langerin$^+$ DC reaching the alveolar lumen. Black pigment deposition is visible. (B,C) Langerin$^+$ DCs displayed a typical dendritic morphology with protrusions extending into the alveolar lumen (arrowhead in B) or a more basolateral position (scale bars in B,C 7 μm). Cell nuclei were counterstained with Mayer's haematoxylin (blue stain). (D,E) Quantification of langerin$^+$ DCs along peripheral lung LAs with squamous and cuboidal interface epithelium. (F) Quantification of the total number of interface langerin$^+$ DCs, including DCs in the columnar interface epithelium. (D–F) Statistical analyses were performed using the Kruskal–Wallis non-parametric test followed by Dunn's multiple comparison post test. Horizontal lines indicate medians for each group. *p<0.05; ***p<0.001. (G) The densities of langerin$^+$ DCs within distinct LA regions. Values are given as mean±SEM.

Correlation with lung function parameters

Several of the parameters associated with the present expansion and remodelling of alveolar–LA interfaces, including the accumulation of interface DCs, correlated inversely with lung function (figure 6 and online supplementary table S2).

DISCUSSION

The present study reveals new aspects of lung LAs in COPD and supports the emerging notion of the alveolar region as a critical site for induction of adaptive immune responses in inflammatory airway diseases. In light of this, the selective accumulation of langerin$^+$ DCs at alveolar–LA interfaces in COPD, which represents a major novel finding in this study, is intriguing and suggests an adaptation for increased alveolar antigen uptake. This adaptation is likely to start early during COPD development because interface DCs were observed in relatively mild disease. Although, for obvious reasons, we could not perform functional studies, it seems evident that the present emergence

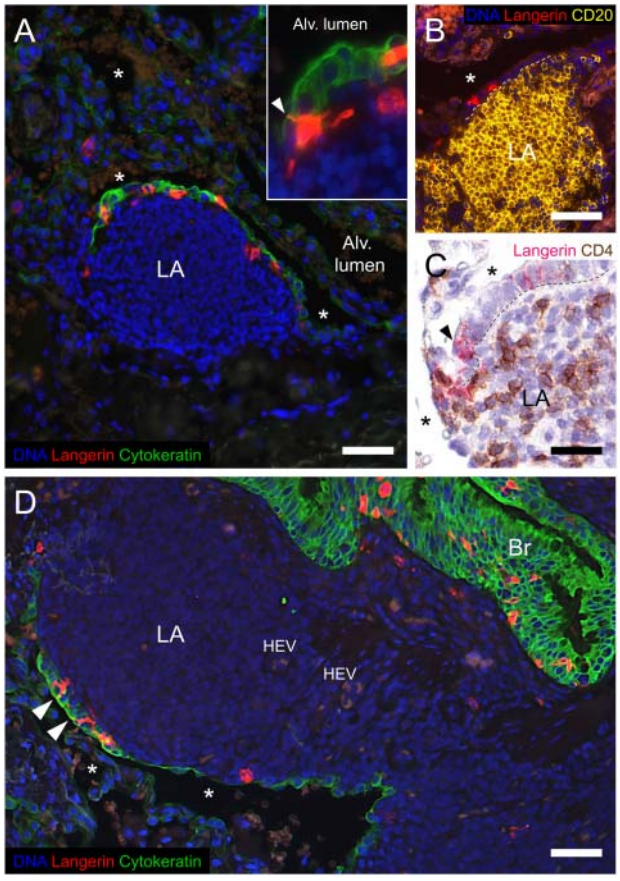

Figure 5 Langerin$^+$ dendritic cells (DCs) colocalised with cytokeratin$^+$ interface epithelium and were in close contact with areas of B and T cells in lymphoid aggregates (LAs). (A) Immunofluorescence double staining revealed colocalisation of langerin$^+$ DCs (red) and cytokeratin$^+$ interface epithelium (green). Langerin$^+$ DCs were in direct contact with (B) CD20$^+$ B cells (yellow) and in close contact with (C) CD4$^+$ T cells (brown). (D) A LA with direct interfaces with the bronchiolar (Br) epithelium and the alveolar lumen*. High endothelial venule (HEV)-like structures were frequently observed within the LAs. All sections were counterstained with DNA-binding fluorochrome (Hoechst 3332, blue). In (A–D), asterisks indicate alveolar lumen. In (A,C,D) arrowheads indicate langerin$^+$ DCs reaching the alveolar lumen. Scale bars: (A,B) 100 μm; (C) 25 μm; (D) 80 μm.

of DC-rich alveolar–LA interfaces in patients with COPD will result in an increased capacity for faster immune responses in the peripheral lung. Indeed, the intimate spatial relationship between the alveolar lymphoepithelial langerin$^+$ DCs and the adjacent T cell areas, and the LAs and extensive network of lymphatic vessels, would create an ideal structural basis for a prompt and highly efficient induction of adaptive immune responses. In this sense the present remodelled LA interface resembles the highly specialised lymphoepithelium overlying the apical part of gut-associated lymphoid tissue (GALT)[22] or classical BALT structures in bronchi.[23] Unfortunately, due to a lack of cell-specific markers, we could not study whether M cells, similar to those present in the lymphoepithelium of GALTs,[22] are also present in the alveolar lymphoepithelium. Theoretically, the occurrence of a higher epithelium at the interfaces could be due to lambertosis (ie, peribronchiolar metaplasia). However, the fact that alveolar columnar epithelium was in the parenchyma exclusively present along the alveolar–lymphoid interfaces suggests that traditional lambertosis is not the major cause of the columnar lymphoepithelium in our study. In any case, regardless of the aetiology of the epithelial changes, it seems clear that the present lymphoepithelium and its selective accumulation of langerin$^+$ DCs represent a novel arena for alveolar antigen uptake. Apart from the release of DC-activating mediators by epithelial cells,[24] physical DC–epithelial interactions are needed to maintain the epithelial barrier when DCs protrude across the tight junctions.[25] Whether this types of interactions are increased in the columnar interface epithelium remains to be established.

Our study also provides the first quantitative data to show that the LAs in COPD are present in all major anatomic regions of the peripheral lung. In agreement, previous studies exploring lung LAs in COPD demonstrated that, apart from BRALTs, LAs were also increased in the alveolar parenchyma.[12–14] However, it has previously been speculated that such seemingly alveolar LAs have physical contact with airways or pulmonary vessels in their three-dimensional in vivo context. Using three-dimensional reconstructions, this study thus proves for the first time that true alveolar-only LAs exist and shows that in COPD these represent around 25% of the total lung LAs. Moreover, this study provides novel quantitative data showing that irrespective of anatomical distribution, the vast majority of the total LAs in COPD lungs have direct interfaces towards the alveolar lumen. Thus, BRALTs and VALTs should conceptually also be viewed as alveolar associated (ie, ALTs). This new view of LAs agrees with previous findings in COPD lungs. For example, van der Strate and colleagues[12] reported that BRALTs very rarely reached the bronchiolar epithelium. In agreement with our study, a similar adventitial distribution has also been noted for VALTs.[26 27] Collectively, it thus seems that an extensive interface towards the alveolar lumen is a general feature of all types of lung LAs.

The origin of the antigens driving the LA formation in COPD is still debated.[11] One source of peripheral antigens comes from lower respiratory tract infections. Apart from the exacerbation-associated infections in COPD,[15] recent microbiome studies reveal a chronic and low-grade presence of lung pathogens outside exacerbations.[28] In addition, inhaled immunogenic microparticles may also induce alveolar adaptive immunity in COPD, as indicated by LA formation in pathogen-free mice exposed to cigarette smoke.[12] Several studies have also demonstrated elevated levels of antibodies to self-antigens.[29 30] Taken together, the antigens captured by the alveolar interface DCs revealed in this study should be expected to be multifaceted. Although the immune responses initiated at alveolar–LA interfaces are likely to have beneficial host defence purposes, it is also likely that in severe COPD these may turn into pathogenic events. It can thus be surmised that, apart from any autoimmune components in COPD, a non-proportional expansion of peripheral alveolar–LA interfaces at advanced stages of COPD results in an 'immunological hyperreactivity' that may evoke harmful and exaggerated immune responses to the frequent infections that hit this patient category.

As for most invasive patient studies, a potential weakness with our study was the limited number of subjects. In part this was compensated by the fact that several separated lung regions (each containing multiple anatomic compartments) were analysed from each patient. In any case, despite restricted patient numbers, robust changes could be observed for the main parameters. In the present study the excised lung samples were immersed into a fixative rather than using a perfusion fixation approach. Although this may result in tissue samples with different degrees of compression, the key parameters in the present study, such as the quantitative analysis of epithelial alterations and degree of DC infiltration along the alveolar–lymphoid

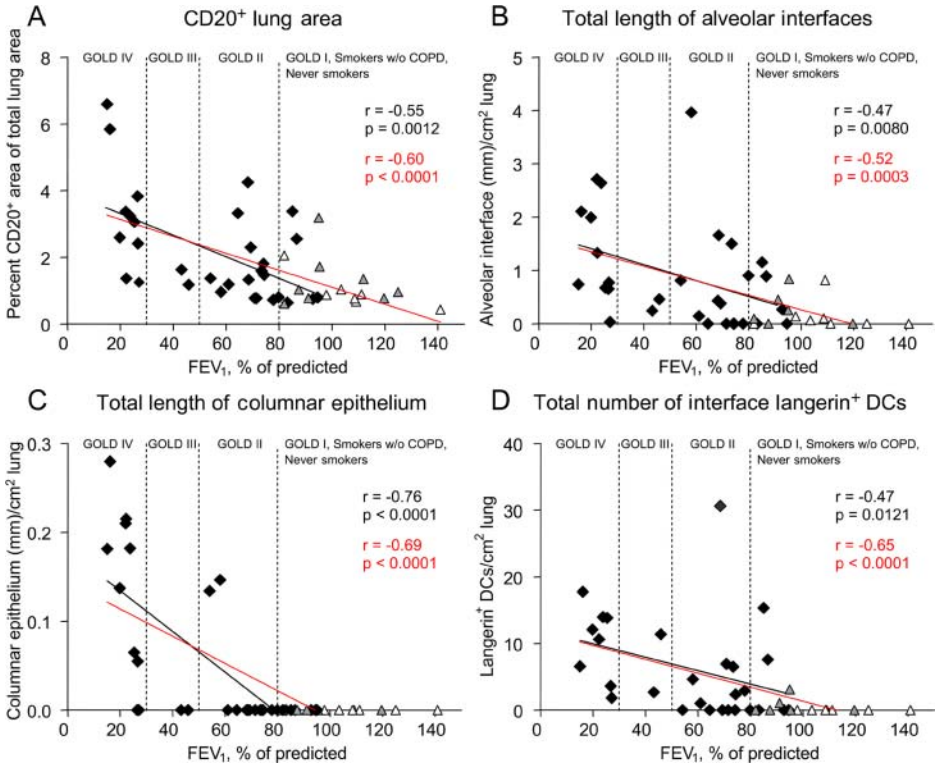

Figure 6 Correlations. There was a negative relationship between forced expiratory volume in 1 s (FEV_1) % of predicted and (A) the total tissue immunoreactivity for CD20, (B) the total length of alveolar interfaces, (C) the total length of columnar interface epithelium, and (D) the total number of interface langerin$^+$ dendritic cells. Black symbols, lines and text represent patients with Global Initiative for Chronic Obstructive Lung Disease (GOLD) stage I–IV chronic obstructive pulmonary disease (COPD). Grey symbols represent smokers without COPD. White symbols represent never smokers. Red lines and text represent all study groups. Spearman's rank correlation was used.

interface, are independent of the degree of compression. Also, it cannot be excluded that suspected cancer in several of our cohorts has influenced the immunological status of the lung. However, since we only included subjects with well delineated bronchial tumours and restricted the analyses to regions far away from the tumour, we believe that any such influence is minimal. Furthermore, the most striking findings were found in patients with GOLD stage IV disease who did not have cancer.

The present findings are expected to have a significant bearing on many other diseases characterised by peripheral lung LAs, for example, long-term distal infections,[31 32] cystic fibrosis[33] and idiopathic pulmonary fibrosis.[32] Notably, patients with autoimmune diseases like idiopathic pulmonary arterial hypertension[27] or rheumatoid arthritis with pulmonary complications[32] develop ectopic lung LAs. Further work is needed to establish if emergence of the DC-rich alveolar–LA interfaces revealed in this study is a general feature of all diseases characterised by lung LAs.

This study may also have important implications for the growing field of pulmonary vaccinology. Respiratory pathogens enter the body at mucosal or alveolar surfaces, but systemically delivered vaccines fail to induce a therapeutic protective response at these sites. This has created a rational for local pulmonary delivery of vaccines to increase lung protection and systemic immunity.[34 35] The novel type of DC-rich alveolar–LA interface shown in this study would likely contribute to an increased efficacy of new and emerging pulmonary vaccine strategies.[36 37]

In summary, this study shows that severity of COPD is associated with a marked remodelling of alveolar–LA interfaces. These alterations, which involve a selective accumulation of interface DCs and correlate with lung function, predict an increased capacity to respond to alveolar antigens and may thus contribute to aggravated inflammation in COPD.

Acknowledgements We thank Karin Jansner and Britt-Marie Nilsson for skilful technical assistance with tissue processing and serial sectioning.

Contributors MM collected tissue samples, performed laboratory work, analysed the data and wrote the manuscript. CKA contributed to tissue handling and sample characterisation. KAS performed three-dimensional reconstructions. PG participated in early preliminary experiments. CGL contributed to the clinical characterisation. JSE designed and supervised the study and wrote the manuscript. All authors participated in manuscript editing and approved the final version of the manuscript.

Funding This work was supported by the Swedish Heart and Lung Foundation and the Swedish Medical Research Council.

Competing interests None.

Ethics approval Ethics approval was provided by the Swedish Research Ethics Committee in Lund.

Provenance and peer review Not commissioned; externally peer reviewed.

REFERENCES

1 Rabe KF, Hurd S, Anzueto A, *et al*. Global strategy for the diagnosis, management, and prevention of chronic obstructive pulmonary disease: GOLD executive summary. *Am J Respir Crit Care Med* 2007;176:532–55.
2 Cosio MG, Saetta M, Agusti A. Immunologic aspects of chronic obstructive pulmonary disease. *N Engl J Med* 2009;360:2445–54.
3 Hogg JC. Pathophysiology of airflow limitation in chronic obstructive pulmonary disease. *Lancet* 2004;364:709–21.
4 Brusselle GG, Joos GF, Bracke KR. New insights into the immunology of chronic obstructive pulmonary disease. *Lancet* 2011;378:1015–26.
5 Jahnsen FL, Strickland DH, Thomas JA, *et al*. Accelerated antigen sampling and transport by airway mucosal dendritic cells following inhalation of a bacterial stimulus. *J Immunol* 2006;177:5861–67.
6 Vermaelen KY, Carro-Muino I, Lambrecht BN, *et al*. Specific migratory dendritic cells rapidly transport antigen from the airways to the thoracic lymph nodes. *J Exp Med* 2001;193:51–60.
7 Hogg JC, Chu F, Utokaparch S, *et al*. The nature of small-airway obstruction in chronic obstructive pulmonary disease. *N Engl J Med* 2004;350:2645–53.
8 Pabst R, Gehrke I. Is the bronchus-associated lymphoid tissue (BALT) an integral structure of the lung in normal mammals, including humans? *Am J Respir Cell Mol Biol* 1990;3:131–5.
9 Aloisi F, Pujol-Borrell R. Lymphoid neogenesis in chronic inflammatory diseases. *Nat Rev Immunol* 2006;6:205–17.
10 Carragher DM, Rangel-Moreno J, Randall TD. Ectopic lymphoid tissues and local immunity. *Semin Immunol* 2008;20:26–42.
11 Brusselle GG, Demoor T, Bracke KR, *et al*. Lymphoid follicles in (very) severe COPD: beneficial or harmful? *Eur Respir J* 2009;34:219–30.

12 van der Strate BW, Postma DS, Brandsma CA, *et al*. Cigarette smoke-induced emphysema: a role for the B cell? *Am J Respir Crit Care Med* 2006;173:751–8.
13 Plumb J, Smyth LJ, Adams HR, *et al*. Increased T-regulatory cells within lymphocyte follicles in moderate COPD. *Eur Respir J* 2009;34:89–94.
14 Polverino F, Baraldo S, Bazzan E, *et al*. A novel insight into adaptive immunity in chronic obstructive pulmonary disease: B cell activating factor belonging to the tumor necrosis factor family. *Am J Respir Crit Care Med* 2010;182:1011–19.
15 Sethi S, Murphy TF. Infection in the pathogenesis and course of chronic obstructive pulmonary disease. *N Engl J Med* 2008;359:2355–65.
16 Thornton EE, Looney MR, Bose O, *et al*. Spatiotemporally separated antigen uptake by alveolar dendritic cells and airway presentation to T cells in the lung. *J Exp Med* 2012;209:1183–99.
17 Veres TZ, Voedisch S, Spies E, *et al*. Spatiotemporal and functional behavior of airway dendritic cells visualized by two-photon microscopy. *Am J Pathol* 2011;179:603–9.
18 Andersson CK, Mori M, Bjermer L, *et al*. Alterations in lung mast cell populations in patients with chronic obstructive pulmonary disease. *Am J Respir Crit Care Med* 2010;181:206–17.
19 Skaland I, Nordhus M, Gudlaugsson E, *et al*. Evaluation of 5 different labeled polymer immunohistochemical detection systems. *Appl Immunohistochem Mol Morphol* 2010;18:90–6.
20 Demedts IK, Bracke KR, Van Pottelberge G, *et al*. Accumulation of dendritic cells and increased CCL20 levels in the airways of patients with chronic obstructive pulmonary disease. *Am J Respir Crit Care Med* 2007;175:998–1005.
21 Van Pottelberge GR, Bracke KR, Demedts IK, *et al*. Selective accumulation of Langerhans-type dendritic cells in small airways of patients with COPD. *Respir Res* 2010;11:35.
22 Corr SC, Gahan CC, Hill C. M-cells: origin, morphology and role in mucosal immunity and microbial pathogenesis. *FEMS Immunol Med Microbiol* 2008;52:2–12.
23 Randall TD. Bronchus-associated lymphoid tissue (BALT) structure and function. *Adv Immunol* 2010;107:187–241.
24 Hammad H, Lambrecht BN. Dendritic cells and epithelial cells: linking innate and adaptive immunity in asthma. *Nat Rev Immunol* 2008;8:193–204.
25 Blank F, Wehrli M, Lehmann A, *et al*. Macrophages and dendritic cells express tight junction proteins and exchange particles in an in vitro model of the human airway wall. *Immunobiology* 2011;216:86–95.
26 Olloquequi J, Montes JF, Prats A, *et al*. Significant increase of CD57+ cells in pulmonary lymphoid follicles of COPD patients. *Eur Respir J* 2011;27:289–98.
27 Perros F, Dorfmuller P, Montani D, *et al*. Pulmonary lymphoid neogenesis in idiopathic pulmonary arterial hypertension. *Am J Respir Crit Care Med* 2012;185:311–21.
28 Sze MA, Dimitriu PA, Hayashi S, *et al*. The lung tissue microbiome in chronic obstructive pulmonary disease. *Am J Respir Crit Care Med* 2012;185:1073–80.
29 Feghali-Bostwick CA, Gadgil AS, Otterbein LE, *et al*. Autoantibodies in patients with chronic obstructive pulmonary disease. *Am J Respir Crit Care Med* 2008;177:156–63.
30 Lee SH, Goswami S, Grudo A, *et al*. Antielastin autoimmunity in tobacco smoking-induced emphysema. *Nat Med* 2007;13:567–9.
31 Suda T, Chida K, Hayakawa H, *et al*. Development of bronchus-associated lymphoid tissue in chronic hypersensitivity pneumonitis. *Chest* 1999;115:357–63.
32 Rangel-Moreno J, Hartson L, Navarro C, *et al*. Inducible bronchus-associated lymphoid tissue (iBALT) in patients with pulmonary complications of rheumatoid arthritis. *J Clin Invest* 2006;116:3183–94.
33 Hubeau C, Lorenzato M, Couetil JP, *et al*. Quantitative analysis of inflammatory cells infiltrating the cystic fibrosis airway mucosa. *Clin Exp Immunol* 2001;124:69–76.
34 Chen K, Cerutti A. Vaccination strategies to promote mucosal antibody responses. *Immunity* 2010;33:479–91.
35 Vujanic A, Wee JL, Snibson KJ, *et al*. Combined mucosal and systemic immunity following pulmonary delivery of ISCOMATRIX adjuvanted recombinant antigens. *Vaccine* 2010;28:2593–7.
36 Nembrini C, Stano A, Dane KY, *et al*. Nanoparticle conjugation of antigen enhances cytotoxic T-cell responses in pulmonary vaccination. *Proc Natl Acad Sci USA* 2011;108:E989–97.
37 Pabst R, Tschernig T. Bronchus-associated lymphoid tissue: an entry site for antigens for successful mucosal vaccinations? *Am J Respir Cell Mol Biol* 2010;43:137–41.

Appearance of Remodelled and Dendritic Cell-Rich Alveolar-Lymphoid Interfaces Provides a Structural Basis for Increased Alveolar Antigen Uptake in Chronic Obstructive Pulmonary Disease

Michiko Mori, Cecilia K. Andersson, Kaj A. Svedberg, Pernilla Glader, Anders Bergqvist, Medya Shikhagaie, Claes-Göran Löfdahl, Jonas S. Erjefält

ONLINE DATA SUPPLEMENT

METHODS

Patients and Lung Tissue Sampling

Patients

Patients were classified as having COPD when FEV_1/(F)VC was less than 70%. The severity of COPD was based on FEV_1% of predicted according to GOLD criteria.[1] Lung tissue from 15 control subjects (never-smokers and smokers), 6 patients with GOLD stage I, 13 patients with GOLD stage II, and 2 patients with GOLD stage III COPD was obtained in relation to surgical resection (lobectomy) for suspected lung cancer.[2] Since it cannot be excluded that the cancer has influenced the immunological status of the lung we, in agreement with similar studies,[3-5]only included patients with a well-delineated bronchial tumour and restricted our analyses to only peripheral tissue as far away from the tumour as possible. Lung tissue from 10 patients with GOLD stage IV COPD was collected from patients requiring lung transplantation.[2] Patients with GOLD stage IV COPD had no history of lung cancer. None of the study subjects had α_1-antitrypsin deficiency. For all patients, the surgical tissue sampling was performed outside any clinical exacerbation.

Peripheral tissue samples and lung compartments investigated for lymphoid aggregates (LAs)

Peripheral tissue samples from randomly selected lobes were subjected to standard fixation with 4% buffered paraformaldehyde. Care was taken to perform the fixation immediately after surgical excision and dissection. Next, the samples were dehydrated and prepared for histological analysis.[2] To allow a more direct comparison between the anatomical parts of the lung, tissue blocks containing bronchioles (non-cartilaginous, <2 mm in internal diameter), pulmonary vessels, and alveolar parenchyma were included in the study (importantly, the selection was performed on blinded sections, and at low power magnification with the sole purpose of assuring the presence of all anatomical regions). A

total of 102 tissue blocks were subjected to detailed analysis: 72 paraffin blocks (two blocks per subject) from controls and patients with GOLD stage I-III COPD, and 30 blocks (three blocks per subject) from patients with GOLD stage IV COPD. In total, among the study groups 978 bronchioles and pulmonary vessels were assessed for LAs. Of these 327 were bronchioles or bronchiole-associated vessels and 651 were solitary pulmonary vessels. There were no differences in numbers of analysed vessels or bronchioles between the study groups. Neither were there any differences in average vessel diameter or bronchiole perimeter between the study groups. For pulmonary vessels only pulmonary arteries, large arterioles, or veins with >140 μm in mean internal diameter were investigated for LAs. The mean vessel diameter was calculated by dividing the sum of the minimal and maximal endothelium-to-endothelium distance by two.

Immunohistochemistry

Prior to immunostaining, four-micron-thick paraffin embedded sections were heated at 60ºC for 20 min, and subjected to simultaneous dewaxing and antigen retrieval according to table 2 (in main manuscript). All staining procedures were performed in an automated slide stainer (Autostainer Plus, DakoCytomation, Glostrup, Denmark). Antibody dilutions were prepared in Dako Antibody Diluent (S0809) and washing steps were performed using Dako Wash Buffer (K8007).

Single staining immunohistochemistry

Sections were immunostained with EnVision™ Peroxidase/DAB Detection System kit (Rabbit/Mouse K5007, Dako, Glostrup, Denmark) according to the manufacturer's instructions. Briefly, endogenous peroxidase activity was blocked for 10 min by 0.3% hydrogen peroxide. The sections were incubated with primary antibodies directed against

CD20, cytokeratin, langerin, BDCA-2, Ki-67 or CD21 (table 2) for 1 h. For BDCA-2 staining, an additional incubation step with EnVision Flex$^+$ Mouse (LINKER) (K8021) for 30 min was performed to amplify the signal of the antibody. All sections were then incubated with Polymer/HRP-linked secondary antibodies and the staining was visualised with 3,3'-diaminobenzidine (DAB) for 10 min. For BDCA-2 staining, sections were incubated with DAB substrate-chromogen solution for 40 min (10 min, four times). Next, sections were rinsed in distilled water and counterstained with Mayer's haematoxylin, dehydrated through ethanol series, cleared in xylene and mounted with Pertex (HistoLab, Gothenburg, Sweden). The specificity of the immunostaining was evaluated by omitting primary antibodies. Immunostaining for CD20, langerin , BDCA-2 or CD21 was performed simultaneously on all tissue sections to avoid variability in staining intensity.

Double staining immunohistochemistry for the identification of lymphatic vessels

Lymphatic vessels were distinguished from smooth-muscle rich blood vessels using double staining immunohistochemistry for podoplanin (lymphatic vessel-specific marker) and α-smooth muscle actin (table 2). All paraffin sections were immunostained simultaneously. Endogenous peroxidase and alkaline phosphatase activity was blocked for 5 min using Dako Dual Endogenous Enzyme Block (S2003). Sections were then incubated for 1 h with antibodies directed against podoplanin, followed by incubation with Polymer/HRP-linked secondary antibodies (Dako EnVision™ Peroxidase/DAB Detection System kit, Rabbit/Mouse K5007). DAB chromogen was used to visualize the binding of the first antibody. Next, sections were incubated with alkaline phosphatase-conjugated anti-α-smooth muscle actin antibodies. The second staining was visualized using Liquid Permanent Red substrate kit (K0640, Dako). After rinsing in distilled water and counterstaining with Mayer's haematoxylin, sections were mounted with Pertex.

Double staining immunohistochemistry for CD4 and langerin expression

Sections were immunostained with antibodies against CD4 using EnVision™ Peroxidase/DAB Detection System kit (Rabbit/Mouse K5007, Dako) as described above. Next, a blocking step with Denaturing Solution (DNS001H, L, Biocare Medical, Concord, CA, USA) for 5 min was performed to prevent additional binding to the first primary antibody. Sections were then incubated with Dako Protein Block Serum Free (X0909) for 10 min, followed by incubation with Dako Avidin/Biotin Blocking kit (X0590) for 10 min. Then sections were incubated with primary antibodies against langerin for 1 h, treated with biotinylated horse anti-mouse IgG secondary antibodies (1:200, BA-2000, Vector Laboratories, Inc., Burlingame, CA, USA), and incubated with Streptavidin-Alkaline Phosphatase (AP) (D0396, Dako). Immunoreactivity was detected with Liquid Permanent Red (K0640, Dako). Next, sections were counterstained with Mayer's haematoxylin and mounted with Pertex.

Double staining immunohistochemistry for CD68 and CD11c expression

Double staining immunohistochemistry for CD68 and CD11c was performed using EnVision™ Gl2 Doublestain System (K5361, Dako) according to the manufacturer's instructions. Endogenous peroxidase and alkaline phosphatase activity was blocked for 5 min. Sections were then incubated with antibodies against CD68, followed by incubation with Polymer/HRP-linked secondary antibodies and DAB substrate-chromogen solution. Next, a blocking step with Doublestain Block Reagent was performed to prevent additional binding of secondary antibodies to CD68 primary antibodies. Next, sections were incubated with antibodies against CD11c and then treated with polymer/AP-linked secondary antibodies. The

immunoreactivity was detected with Liquid Permanent Red. Finally, sections were counterstained with Mayer's haematoxylin and mounted with Pertex.

Double staining immunofluorescence

Immunofluorescence was performed to investigate colocalization of langerin$^+$ DCs and cytokeratin$^+$ epithelial cells, and colocalization of langerin$^+$ DCs and CD20$^+$ B-cells. Sections were blocked for 10 min with Dako Protein Block Serum Free solution (X0909) to reduce non-specific binding. An additional blocking step with Dako Avidin/Biotin Blocking kit (X0590) for 10 min was performed, followed by incubation for 1 h with primary antibodies directed against langerin. Sections were then incubated for 1 h with biotinylated horse anti-mouse IgG secondary antibodies (1:200, BA-2000, Vector Laboratories), followed by 30 min incubation with Streptavidin-Alexa Fluor 555 (1:100, S32355, Life Technologies^{TM}/Molecular Probes$^{®}$, Eugene, OR, USA). Next, a blocking step with Denaturing Solution (DNS001H, L, Biocare Medical) for 5 min was performed to prevent additional binding of secondary antibodies to the first primary antibody. A second incubation for 1 h with primary antibodies directed against cytokeratin or CD20 was performed and antibody binding was detected by secondary Alexa Fluor 488 conjugated goat anti-mouse IgG antibodies (1:200, A11001, Life Technologies^{TM}/Molecular Probes$^{®}$). Hoechst (H33342) was used as nuclear staining. Finally, sections were mounted in PBS/glycerine and examined using Nikon Eclipse 80i microscope (Nikon Instruments, Japan).

Serial Section-Based Three-Dimensional Reconstruction of LAs

Four-micron-thick serial sections (>400) were stained with Mayer's haematoxylin-eosin. Digital images of whole sections were generated with ScanScope Slide Scanner (20x/40x objective, Aperio Technologies). LAs in 32 consecutive sections were manually traced. Images were captured using Aperio ImageScope software (Aperio Technologies) and saved to

an image stack of lossless .tiff file format. Registration and segmentation was done using Adobe® Photoshop CS 4™. The original image stack was registered by manually aligning consecutive slides. Segmentation was done by each LA of interest first being marked by histogram colour segmentation and then manually separated out of the original image and saved to a separate binary black and white file. The binary images for each segmented structure were then all reduced equally in image size maintaining aspect ratios and introduced as separate binary stacks into Amira® 5.4.2 Visage Imaging® (Visage Imaging Inc., San Diego, CA, USA). The 3D images were generated by overlaying each separate structure's binary stack into the final composite image, maintaining X, Y, Z ratios between the stacks and adjusting for the section thickness in the Z voxel size. Similarly, series with 40 (four-micron-thick) serial sections stained with podoplanin antibodies was used to visualize the 3D relationship between lymphatic vessels, alveolar-LA interfaces and LAs.

Quantifications

High-resolution digital images of whole lung tissue were generated from all bright-field sections using ScanScope Slide Scanner (Aperio Technologies) and morphometric analyses were performed using Aperio ImageScope software (Aperio Technologies). All quantifications involving manual counting or manual cursor tracing was performed on blinded sections.

Number of LAs

The number and anatomical distribution of LAs were quantified on Masson's trichrome-stained sections. On each section the perimeter of the whole lung tissue (including bronchioles, pulmonary vessels, parenchymal tissue, and airspaces) was manually traced and the corresponding cross-sectional area was expressed as square centimetre of the total

peripheral lung tissue. In all sections, the total number of LAs was counted and data were expressed as number of LAs per square centimetre of peripheral lung. Similarly, the number of LAs in the different lung compartments (i.e. small airway/bronchiolar- (BRALT), vascular- (VALT), and alveolar-only (ALT) associated aggregates) were counted and expressed as number of LAs per square centimetre of peripheral lung.

Cross-sectional area of LAs

The area of individual LAs was quantified on Masson's trichrome-stained sections. On each section LAs were manually delineated and the number of pixels corresponding to the cross-sectional LA area was counted and expressed as square millimetre of the LA. The total cross-sectional area of all identified LAs in one section was calculated and data were expressed as the percentage of the LA area per total lung area.

Total CD20 immunoreactivity in whole sections

On each section, the perimeter of the whole lung tissue was delineated and a pixel threshold was selected to only include positive immunostained pixels (brown colour of DAB), representing CD20 immunoreactivity (Aperio Positive Pixel Count Algorithm v.9, Aperio Technologies). In the selected area, the total number of immunopositive pixels above the selected threshold level and the total number of pixels (i.e. immunopositive and negative) were used to calculate the percentage of the total lung area occupied by CD20-staining.

Alveolar-LA interfaces and surrounding anatomic structures

The number of LAs with a direct interface towards the alveolar lumen was quantified on podoplanin/α–smooth muscle actin-stained sections. The length of the alveolar-LA interface was measured by manual cursor tracing. The total length of alveolar-LA interfaces was

calculated for each section by multiplying the mean length of the alveolar interfaces (expressed in millimetres) by the number of LAs per square centimetre of peripheral lung. Data were expressed as the total length of alveolar interfaces per square centimetre of peripheral lung.

The length of podoplanin$^+$ lymphatic vessels was measured by delineating only the part of the podoplanin$^+$ vessel that surrounded the LA (i.e. podoplanin$^+$ vessels within the LAs were excluded from the analysis). In addition to the alveolar lumen and lymphatic vessels, LAs were surrounded by airway wall compartments, the adventitia layer of pulmonary vessels and/or interstitial tissue, all of which were termed "tissue". The length of each LA-associated structure, divided into alveolar interface, lymphatic vessel, or remaining firm tissue, was used to quantify the relative proportion of each anatomic structure along the LA perimeter.

The epithelium at alveolar-LA interfaces

In LAs with alveolar interfaces, the length of the interface epithelium was measured by manually tracing each type of epithelium (i.e. simple squamous, simple cuboidal or non-ciliated columnar epithelium). The proportion of squamous, cuboidal, or columnar epithelium was expressed as the percentage of the total alveolar interface length. The total length of the columnar interface epithelium was calculated for each section by multiplying the mean length of the columnar epithelium (expressed in millimetres) by the number of LAs per square centimetre of peripheral lung. The results were expressed as the total length of columnar epithelium per square centimetre of peripheral lung.

Langerin$^+$ DCs

Langerin$^+$ DCs within LAs (including the alveolar-LA interfaces) were manually counted and

expressed as number of langerin$^+$ DCs per square millimetre of LA. In LAs with alveolar interfaces, the number of langerin$^+$ DCs along squamous, cuboidal or columnar interface epithelium was counted and the data were expressed as the number of DCs per millimetre length of the interface epithelium. Similarly, the numbers of BDCA-2$^+$ plasmacytoid and CD68$^-$CD11c$^+$ myeloid DCs were quantified along the alveolar-LA interfaces. The total number of interface langerin$^+$ DCs (including squamous, cuboidal and columnar interface epithelium) was calculated on each section by multiplying the mean number of langerin$^+$ DCs per millimetre alveolar interface by the number of LAs per square centimetre of peripheral lung. Data were expressed as the total number of interface langerin$^+$ DCs per square centimetre of peripheral lung.

In LAs with alveolar interfaces, the number of langerin$^+$ DCs was quantified in three separate regions within the LAs: the superficial region, defined as the region within a distance of 20 µm beneath the alveolar-LA interface; the central part of the LA; the opposing region, defined as the region within a distance of 20 µm beneath the boarder of surrounding firm tissue. The area of the superficial region was calculated by multiplying the length of the alveolar interface by 20 µm and data were expressed as number of DCs per square millimetre of the superficial region. The number of DCs in the central part of the LA was counted within a grid (20 µm x 98 µm) and the data were expressed as average number of DCs per square millimetre grid area. The area of the opposing region was calculated by multiplying the length of the tissue boarder by 20 µm and data were expressed as number of DCs per square millimetre of the opposing region.

RESULTS

Patients

A complete medical history was obtained from 9 out of 10 patients in the GOLD stage IV-group. There was no difference in age between control subjects and patients with COPD ($p>0.05$). Moreover, there was no difference in pack-years between smokers without COPD and patients with COPD ($p>0.05$).

General Expansion and Characteristics of LAs in Advanced Stage COPD

Peripheral lung LAs were observed in all study groups (figure S1A and table S1). Advanced COPD was associated with both increased number of LAs per tissue area and percentage of the total lung tissue occupied by LAs compared with never-smoking control subjects (figure S1A,B). There was no difference in the mean cross-sectional area of LAs between the control and COPD groups (table S1). Since the vast majority of the $CD20^+$ B-cells in COPD lungs are localized to LAs (exemplified in figure S1D), total tissue $CD20^+$ cells was used as complementary marker of lung LAs. Also this parameter increased in advanced COPD (figure S1C).

Cells positive for the proliferation antigen Ki-67 and CD21, a marker of follicular DCs, (figure S2) were used as indices of maturation and activation status of the lung LAs. The percentage of LAs containing $CD21^+$ follicular DCs was significantly increased in patients with GOLD stage IV COPD (median, 100%; range, 53-100%) compared with never-smoking controls (median, 20%; range, 0-50%; $p=0.006$). Although the expression of Ki-67 was not quantified, it was evident that clusters of Ki-67^+ cells were commonly observed among the LAs.

Importantly, neither the numbers of BDCA-2^+ plasmacytoid, nor $CD68^-CD11c^+$ myeloid DCs were found to have similar spatial association to alveolar-lymphoid interfaces as the langerin$^+$ DCs (figure S3).

FIGURE LEGENDS

Figure S1. Expansion of peripheral lymphoid aggregates (LAs) in patients with COPD. (*A*) The total number of LAs and (*B*) the total cross-sectional area of LAs were quantified on Masson's trichrome-stained sections from peripheral lung samples obtained from never-smokers, smokers without COPD and patients with GOLD stage I-IV COPD. (*C*) Quantification of the total tissue immunoreactivity for $CD20^+$ B-cells. (*A-C*) Statistical analyses were performed using Kruskal-Wallis nonparametric test followed by Dunn's multiple comparison post-test. Horizontal lines indicate medians for each group. *: $p<0.05$; **: $p<0.01$. (*D*) The vast majority of $CD20^+$ B-cells (*brown* colour) were located within scattered LAs that were distributed throughout the distal lung, including (*E*) bronchioles (Br), (*F*) pulmonary vessels (PV, black pigment deposition is visible), and (*G*) the alveolar parenchyma. Cell nuclei were counterstained with Mayer's haematoxylin (*blue* stain). *Scale bars*: (*D*) 1000 µm; (*E-G*) 100 µm.

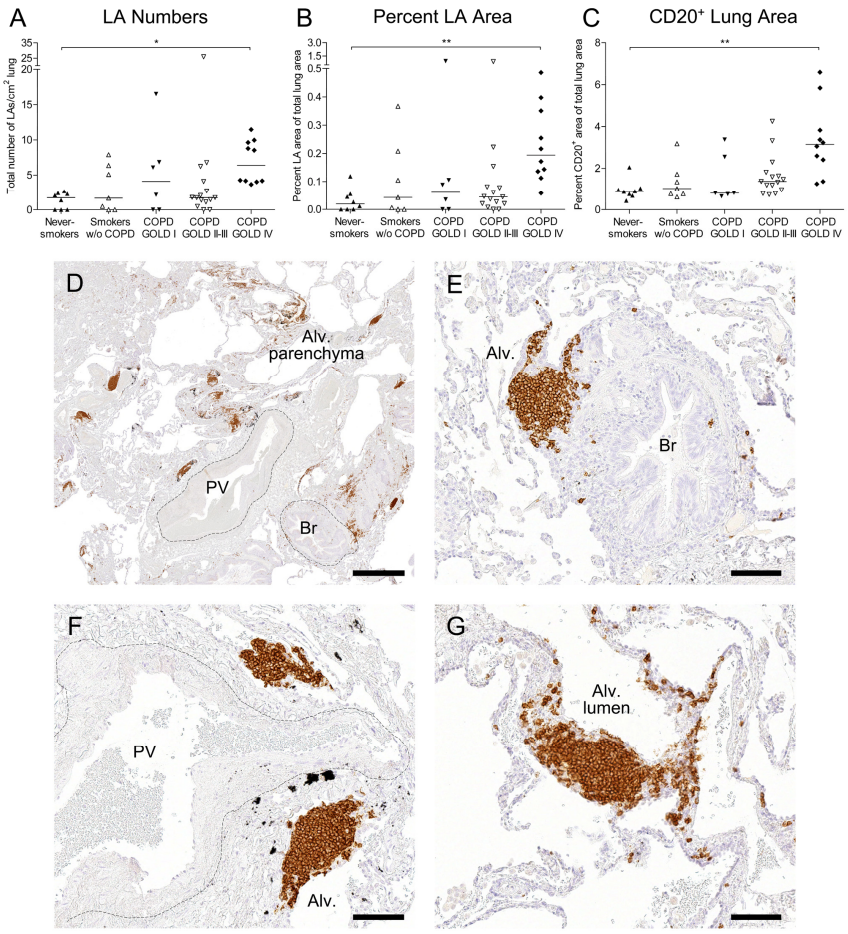
A
LA Numbers
Total number of LAs/cm² lung
B
Percent LA Area
Percent LA area of total lung area
C
CD20⁺ Lung Area
Percent CD20⁺ area of total lung area
Never-smokers
Smokers w/o COPD
COPD GOLD I
COPD GOLD II-III
COPD GOLD IV
D
Alv. parenchyma
PV
Br
E
Alv.
Br
F
PV
Alv.
G
Alv. lumen

Figure S2. Characterisation of lymphoid aggregates (LAs) in patients with GOLD stage IV COPD. (*A*) Ki-67^{+} proliferating cells (shown in *brown* colour) were frequently present in the LA centres (i.e. germinal centres). *(B)* CD21^{+} follicular dendritic cells (*brown* colour) formed a network within the LAs. *(C)* A higher magnification of the CD21^{+} follicular dendritic cell network. Cell nuclei were counterstained with Mayer's haematoxylin (*blue* stain). *Scale bars*: (*A-B*) 150 µm; *(C)* 50 µm.

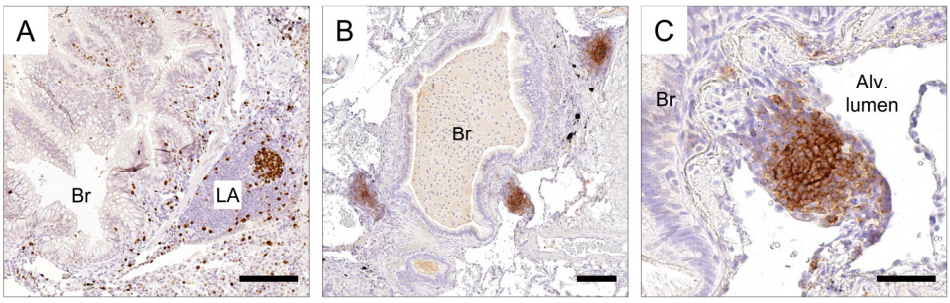

Figure S3. Comparisons between dendritic cell (DC) subsets along alveolar-lymphoid aggregate (LA) interfaces. (*A*) Quantification of the numbers of BDCA-2$^+$ plasmacytoid DCs, CD68$^-$CD11c$^+$ myeloid DCs, and langerin$^+$ DCs along the alveolar-LA interfaces. Values are given as mean ± SEM. *(B)* Photomicrograph exemplifying the distribution of BDCA-2$^+$ plasmacytoid DCs (*brown* colour) in LAs. Black pigment deposition is visible. *(C)* Photomicrograph exemplifying CD68$^+$ monocytes/macrophages (*brown* colour) and CD68$^-$ CD11c$^+$ myeloid DCs (*red* colour) in LAs. Cell nuclei were counterstained with Mayer's haematoxylin (*blue* stain). *Scale bars*: (*B*-*C*) 50 µm.

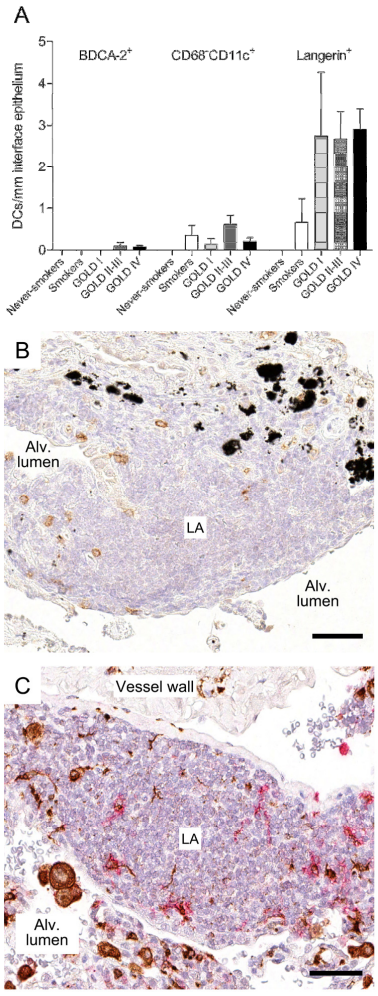

TABLES

TABLE S1. CHARACTERISTICS OF LYMPHOID AGGREGATES IN DIFFERENT ANATOMICAL COMPARTMENTS OF PERIPHERAL LUNG

Parameters	Never-smokers	Smokers w/o COPD	GOLD I COPD	GOLD II-III COPD	GOLD IV COPD	Overall p-value*
Subjects with LAs (yes/no)	5/3	5/2	4/2	13/2	10/0	0.249
Number of LAs per cm^2 of total lung						
BRALT	0.51 (0-2.27)	0.85 (0-6.37)	0.51 (0-4.86)	0.55 (0-6.17)	2.67 (0.40-3.98)	0.071
VALT	0 (0-0.42)	0 (0-2.55)	0.51 (0-6.80)	0 (0-1.24)	1.35 (0.43-3.27) †† ‡‡	0.001
ALT	0 (0-1.81)	0 (0-5.27)	1.92 (0-4.86)	1.16 (0-18.52)	3.21 (0.76-5.05)	0.052
Total LA area, % of total lung area						
BRALT	0.01 (0-0.09)	0.02 (0-0.21)	0.01 (0-0.10)	0.01 (0-0.24)	0.10 (0.01-0.18) ‡	0.027
VALT	0 (0-0.01)	0 (0-0.08)	0.01 (0-0.21)	0 (0-0.05)	0.06 (0.01-0.15) †† ‡‡	0.001
ALT	0 (0-0.02)	0 (0-0.22)	0.03 (0-0.61)	0.03 (0-0.59)	0.05 (0.02-0.16) †	0.021
Cross-sectional area of LAs, mm^2						
All LAs	0.02 (0.01-0.04)	0.03 (0.01-0.05)	0.02 (0.01-0.16)	0.02 (0.01-0.04)	0.03 (0.02-0.17)	0.246
BRALT	0.02 (0.01-0.08)	0.03 (0.02-0.05)	0.01 (0.01-0.02)	0.03 (0.01-0.04)	0.03 (0.01-0.05)	0.318
VALT	0.01 (0.01-0.03)	0.04 (0.02-0.06)	0.02 (0.01-0.10)	0.04 (0.01-0.05)	0.04 (0.02-0.06)	0.370
ALT	0.02 (0.01-0.02)	0.02 (0.01-0.04)	0.02 (0.01-0.34)	0.02 (0.02-0.05)	0.03 (0.01-0.05)	0.608

Values are median (range), unless specified by n.
* Kruskal-Wallis test for differences between groups. Dunn's multiple comparisons post-test: † $p<0.05$ compared with never-smokers; †† $p<0.01$ compared with never-smokers; ‡ $p<0.05$ compared with GOLD stages II-III COPD; ‡‡ $p<0.01$ compared with GOLD stages II-III COPD.
ALT, alveolar-only lymphoid tissue; BRALT, small airway/bronchiolar-associated lymphoid tissue; COPD, chronic obstructive pulmonary disease; GOLD, Global Initiative for Chronic Obstructive Lung Disease; LA, lymphoid aggregate; VALT, vascular-associated lymphoid tissue.

TABLE S2. CORRELATIONS TO FEV_1/(F)VC*

Variable	All COPD Subjects	
	r-value	p-value
Total length of alveolar interfaces (mm) per cm^2 lung	-0.46	0.010
Total length of columnar epithelium (mm) per cm^2 lung	-0.70	<0.001
Percent $CD20^+$ area of total lung area	-0.46	0.009
Total number of interface $langerin^+$ dendritic cells per cm^2 lung	-0.49	0.008

* Spearman's rank correlation was used.
COPD, chronic obstructive pulmonary disease; FEV_1, forced expiratory volume in one second; (F)VC, (forced) vital capacity.

REFERENCES

1. Rabe KF, Hurd S, Anzueto A*, et al.* Global strategy for the diagnosis, management, and prevention of chronic obstructive pulmonary disease: GOLD executive summary. *Am J Respir Crit Care Med* 2007;**176**:532-55.

2. Andersson CK, Mori M, Bjermer L*, et al.* Alterations in lung mast cell populations in patients with chronic obstructive pulmonary disease. *Am J Respir Crit Care Med* 2010;**181**:206-17.

3. Polverino F, Baraldo S, Bazzan E*, et al.* A novel insight into adaptive immunity in chronic obstructive pulmonary disease: B cell activating factor belonging to the tumor necrosis factor family. *Am J Respir Crit Care Med* 2010;**182**:1011-19.

4. van der Strate BW, Postma DS, Brandsma CA*, et al.* Cigarette smoke-induced emphysema: A role for the B cell? *Am J Respir Crit Care Med* 2006;**173**:751-8.

5. Van Pottelberge GR, Bracke KR, Van den Broeck S*, et al.* Plasmacytoid dendritic cells in pulmonary lymphoid follicles of patients with COPD. *Eur Respir J* 2010;**36**:781-91.